

1 **Rapid duplexed detection of illicit drugs in wastewater using gold**
2 **nanoparticle conjugated aptamer sensors**

3 Kang Mao^a, Jun Ma^b, Xiqing Li^a, and Zhugen Yang^{c*}

4 ^a *Laboratory for Earth Surface Processes, College of Urban and Environmental*
5 *Sciences, Peking University, Beijing 100871, China*

6 ^b *Guangzhou Huali Science and Technology Vocational College, Guangzhou, 511325,*
7 *China*

8 ^c *School of Water, Environment and Energy, Cranfield University, Cranfield, MK43*
9 *0AL, United Kingdom*

10 Corresponding Email: zhugen.yang@cranfield.ac.uk (Dr Z. Yang)

11 **Abstract:** The abuse of illicit drug addiction is a worldwide public health and social
12 problem. In this paper, we reported on a simple and rapid colorimetric biosensor for
13 duplexed detection of methamphetamine (METH) and cocaine in a single assay. Gold
14 nanoparticles (AuNPs) and Au@Ag NPs were synthesized and functionalized with
15 DNA reporter probes (RPs) for METH and cocaine, respectively. The magnetic beads
16 (MBs) were conjugated with two capture probes (CPs) respective to METH and
17 cocaine. The respective RPs and CPs were designed to hybridize with each illicit
18 drug-binding DNA aptamers through DNA-DNA hybridization, forming a sandwich
19 structure. This MBs-based sandwich structure could be removed with an external
20 magnetic field. However, due to the higher affinity of DNA aptamers with illicit
21 drugs, the sandwich structure was disassembled when illicit drugs are introduced into
22 the solution, leading to the colour changes of the supernatant. Utilizing a non-negative
23 matrix factorization (NMF) algorithm to process the data, we demonstrated the ability

24 of our biosensor for the simultaneous quantification of two illicit drugs. Under the
25 optimal condition, our sensors were able to detect both METH and cocaine at the nM
26 level with a wide dynamic range. This sensing platform provides a huge potential on
27 drug consumption evaluation at the community level for wastewater-based
28 epidemiology.

29 **Keywords:** illicit drug of abuse, wastewater-based epidemiology, colorimetric
30 biosensor

31 1. **Introduction**

32 Illicit drug abuse has become a global concern considering its close relationship
33 with the increasing incidence of crimes and severe social problems (Cyranoski, 2018;
34 Galanie et al., 2015; Merz, 2018). Methamphetamine (METH) and cocaine (COC)
35 and are two of the most widely abused illegal drugs in the world (EMCDDA, 2016;
36 Merz, 2018; Mokhtarzadeh et al., 2015; Xu et al., 2017). To evaluate the pattern of
37 illicit drug consumption, a new approach namely wastewater-based epidemiology
38 (WBE) has emerged in the past decade. Usually, the drug residues and their
39 metabolites would be excreted by humans in a given area (e.g., a city and a
40 community) pool in wastewater at a certain wastewater treatment plants. WBE is
41 conducted by collecting wastewater samples and analysing the concentration of
42 targets in wastewater, and thereby can be used to monitor the community-wide drug
43 consumption taking into account population served, stability of drug residues,
44 excretion rates, and wastewater volumes (Cyranoski, 2018; Du et al., 2017; Du et al.,
45 2018; van Nuijs et al., 2011; Zuccato et al., 2005). Compared to the conventional
46 population survey method, WBE holds several advantages such as more objective and
47 much less time-consuming (Du et al., 2018; Ettore et al., 2008), and thus this strategy

48 has been widely used for the monitoring of illicit drugs in many countries (Du et al.,
49 2017; EMCDDA, 2016; Thomas et al., 2012), including America (Foppe et al., 2018),
50 Australia (Bade et al., 2019) and many European countries (Castrignanò et al., 2018;
51 EMCDDA, 2016). To get the concentration of wastewater, the widely employed
52 analytical instrument is mass spectrometry (MS) coupled with high-performance
53 liquid chromatography (HPLC), which is robust, highly sensitive and selective (Du et
54 al., 2015; Gao et al., 2017). But these methods usually need a sample preparation
55 before illicit drug analysis, such as the purification of raw wastewater with solid phase
56 extraction. In addition, the compulsory sample preparation usually requires the well-
57 trained personnel to operate an instrument for analysis and then interpret the data in
58 the central laboratory. In order to evaluate illicit drugs of abuse, preferably at the site
59 of sample collection, there is an urgent need to develop rapid, simple and inexpensive
60 tools for detection illicit drugs in complex environmental samples.

61 As an rapid and cost-effective analytical tool, aptamer biosensor (aptasensor) has
62 attracted increasing attention for determination of illicit drugs, such as cocaine,
63 methamphetamine, codeine and ketamine (Asghary et al., 2018; Lodha et al., 2014;
64 Mao et al., 2018; Mokhtarzadeh et al., 2015; Roncancio et al., 2014). The signal of
65 sensors from the binding between DNA aptamers and illicit drugs can be detected
66 with colorimetry (Li et al., 2013), fluorescence (Stojanovic et al., 2000) and Surface-
67 Enhanced Raman Spectrometry (SERS) (Mao et al., 2018), electrochemistry (Yang et
68 al., 2016), and other techniques (Neves et al., 2015; Ya et al., 2015). We have recently
69 developed electrochemical aptamer sensors for the determination of cocaine in
70 wastewater, which demonstrated the cocaine consumption trends with a weekend
71 peak based on the sampling in a wastewater treatment plant in the Southwest of
72 England (Yang et al., 2016). For METH determination, we have developed a new

73 colorimetric strategy using G-quadruplex DNAzyme for the determination of METH
74 (Mao et al., 2016). Although these assays mentioned above show the great capability
75 for single illicit drug determination, there are no reports on biosensors for
76 simultaneous determination of multiple illicit drugs so far. In fact, a variety of illicit
77 drugs (such as METH, cocaine, et al.) are usually present in the sample at the same
78 time, which are widely distributed and transported in natural water and wastewater
79 (EMCDDA, 2016). Although one can use several biosensors for the determination of
80 various targets separately, it is costly and time-consuming. Thus, there is a great need
81 for the development of simultaneous determination of multiplexed illicit drugs within
82 a single assay. This may provide opportunities for the monitoring of illicit drugs at a
83 trace level in the environment matrixes.

84 The rapid development of nanomaterial-related technologies (Tang et al., 2018)
85 provides a huge opportunity for designing selective and sensitive aptasensors for the
86 determination of illicit drugs. For example, recent development and applications of
87 nanomaterial-based illicit drug aptasensors by using optical and electrochemical
88 analytical techniques for illicit drugs determination have been reviewed (Kumar et al.,
89 2018; Mokhtarzadeh et al., 2015). In these nanomaterials, AuNPs has been widely
90 used to improve the sensitivity due to their unique properties such as facile
91 preparation methods and excellent optical properties (Shen et al., 2010; Xie et al.,
92 2011). Magnetic beads, have been widely applied for determination and separation
93 due to their wonderful magnetic separation characteristics, excellent binding kinetics,
94 good maneuverability, and biological targeting properties (Song et al., 2014; Wen et
95 al., 2014). However, to our knowledge, the analytical method based on the
96 combination of gold nanoparticles and MBs for the multiplexed determination of
97 illicit drugs has not yet been reported.

98 Hence, we designed a new biosensing strategy for the simultaneous multiplexed
99 determination of illicit drugs in a single assay, which offers a rapid signal response of
100 targets through simply mixing DNA aptamers for signal readout. Our platform based
101 on non-aggregated AuNPs together with magnetic beads displayed high selectivity
102 and sensitivity towards the targets, which holds unique advantages by comparing
103 classical colorimetric method and could be extend for more wide application. Because
104 AuNPs coated with silver-Au@Ag show similar determination capability with AuNPs
105 but with different optical signals, we combined Au@Ag NPs with AuNPs together to
106 develop a colorimetric system for multiplexed determination of METH and cocaine.
107 In order to prevent ambiguities related to colour determination by visual assay, we
108 introduced a data algorithm analysis system based on functional non-negative matrix
109 factorization (NMF) for targets quantification, which was consistent with the
110 colorimetric result. According to this finding, the feasibility of non-aggregated metal
111 NPs colorimetric determination of two illicit drugs in a single assay was demonstrated
112 for the first time. We believed that colorimetric analysis based on the combination of a
113 non-aggregated noble metal nanoparticle and NMF analysis has a huge potential as a
114 generic platform for the multiplexed determination of a variety of targets.

115 **2. Materials and Methods**

116 **2.1. Materials**

117 All oligonucleotide sequences were purified by HPLC and ordered from Sangon
118 Biotech Co. Ltd. (Shanghai, China) (detailed in Table S1). Carboxyl-modified
119 magnetic beads (MBs, 1.05 μm DynabeadsTM My OneTM, 10 mg mL⁻¹) were bought
120 from Thermo Fisher Scientific. Chloroauric acid (HAuCl₄·3H₂O) and silver nitrate
121 (AgNO₃) were ordered from Shanghai Chemical Reagent (Shanghai, China) Co., Ltd.
122 All illicit drugs and metabolites, including METH and cocaine were bought from

123 Cerilliant (Round Rock, USA). The ultrapure water is purified using a Millipore
124 filtration system (18.2 MΩ·cm) in the whole experiments. All experiments were
125 performed in compliance with the relevant laws and institutional guidelines, and all
126 reagents in this experiment have been agreed by the institutional committee (Peking
127 University, the People's Republic of China).

128 **2.2. Instrumentation**

129 A Scanning Electron Microscope (SEM) (ZEISS, SIGMA) was used to obtain the
130 SEM pictures of AuNPs and Au@Ag. A JEM-2100 (HR, Japan) microscope was
131 utilized to obtain the TEM images of AuNPs and Au@Ag NPs. UV-vis spectra of
132 AuNPs and Au@Ag were recorded by Lambda 35 UV-vis spectrometer (Perk Elmer,
133 USA) through 80 μL quartz cells with a path length of 1 cm.

134 **2.3. Synthesis of AuNPs and Au@Ag**

135 In this experiment, AuNPs stabilized by citrate were synthesized as follows: 50 mL
136 HAuCl₄ (0.01%, w/w) was reduced by addition 750 μL trisodium citrate (1%, w/w) at
137 120 °C using magnetic stirring for 25 minutes until the obtained reaction mixtures
138 turned to be wine red. Au@Ag NPs were synthesized in a seed-mediated method
139 following the previous report (Shen et al., 2010). Firstly, 600 μL 0.5 % (w/w) AgNO₃
140 solution was introduced to boiling gold seed solution (100 mL). Then, 1 mL 1 %
141 (w/w) sodium citrate solution as the reducing agent was introduced dropwise under
142 stirring. The mixture was boiled for 1 h and Au@Ag was ready to use after cooling
143 down.

144 **2.4. The preparation of RPs and CPs**

145 The RPs were prepared as follows: The two types of NPs were conjugated with the
146 different RP DNA sequences by treating citrate-stabilized nanoparticles with a
147 solution containing thiol-modified oligonucleotides, respectively (Figure S1A). 15

148 nmol thiolated RP DNA sequence was introduced to 5 ml Au@Ag NPs or AuNPs
149 nanoparticles suspended in PB buffer. After 24 h incubation, 2 M NaCl was
150 introduced to reach the salt concentration at 0.05 M and then increased to 0.1 M after
151 standing for 8 h. The nanoparticles were isolated through centrifugation and washed
152 with PBS-T solution after aging in 0.1 M NaCl for two days.

153 The CPs were prepared as follows: The carboxylated MBs were conjugated with
154 the CP DNA following the manufacturer's protocol. 2.5 mL carboxylated MBs were
155 washed two times with 2.5 mL MES solution and the MBs were re-suspended in 250
156 μ L MES buffer before immobilization. The mixture of 36.2 nmol amino-modified CP
157 DNA and 36.2 μ mol EDC HCl was introduced to MBs solution and incubated at 25 °C
158 by gently shaking overnight. In the end, to quench excess activated carboxylic acid
159 groups on the surface of MBs, the MBs were incubated with 50 mM Tris solution for
160 15 minutes at 25 °C by gently shaking. The coated MBs were washed three times
161 using 2.5 mL Tris solution and then re-suspended in PBS-T solution for use.

162 **2.5. Elaboration and optimization of biosensors**

163 **2.5.1. Elaboration of biosensors**

164 As shown in Scheme 1, this sensing platform consisted of a CP, RP and an
165 aptamer. The aptamer bound CP and RP through hybridization forms a double-
166 stranded DNA (dsDNA). After removing Au@Ag NPs-DNA-MBs or AuNPs-DNA-
167 MBs complex by an external magnetic field, we can observe a decreased absorbance
168 signal of Au@Ag solution. However, the target illicit drugs can prevent the formation
169 of dsDNA due to a higher affinity between the targets and the designed aptamer. The
170 dose of illicit drugs could generate a different signal that can be measured by a UV-
171 vis spectrometer.

172 To evaluate the feasibility of the biosensing mechanism, a typical non-aggregated

173 Au@Ag nanosensor for METH determination was acted as a case study. 5 μL METH
174 (cocaine, 5 μM) was mixed with 5 μL of 1.2 μM METH aptamer (or 1 μM cocaine
175 aptamer) solutions, followed through adding 20 μL PBS-T solution. After incubation
176 for 30 minutes, 1 μL CP and 50 μL RP were introduced to the mixture and then
177 hybridized reaction with gentle shaking for 90 minutes. The total volume was kept at
178 150 μL by added PBS-T solution. After hybridization reaction, the magnetic beads
179 with target-linked AuNPs or Au@Ag NPs together with unreacted MBs were
180 removed by using an external magnetic field. We can measure the supernatant for
181 signal readout after the separation by a UV-vis spectrometer in 80 μL quartz micro-
182 cuvette at 25 $^{\circ}\text{C}$.

183 We also carried out control experiments with following mixtures: CP and RP; CP,
184 RP, and illicit drug; CP, RP, and aptamer. In our experiment, each component was
185 introduced as the same volume and concentration as in the presence of METH or
186 cocaine. A certain volume of PBS-T solution was added into the mixture to obtain a
187 150 μL constant volume in total.

188 **2.5.2. Optimization of the determination conditions**

189 The MBs concentration had a significant effect on the sensitivity of the assay
190 because the ratio between the CPs and RPs would change. To ensure a highly
191 sensitive analysis, a series of MBs concentration from 3.3 $\mu\text{g L}^{-1}$ to $3.3 \times 10^2 \mu\text{g L}^{-1}$
192 (3.3, 6.6, 3.3×10^1 , 6.6×10^1 and $3.3 \times 10^2 \mu\text{g L}^{-1}$) were tested under the same
193 conditions to get the optimal concentration of the MBs.

194 The hybridization time was also a significant parameter for colorimetric assay. The
195 hybridization time was studied through measuring the peak intensities of UV-vis
196 spectra. The time interval was recorded 15 minutes a time ranging 0-105 minutes.

197 The optimal METH aptamer concentration which may influence the UV-vis spectra

198 of Au@Ag NPs and AuNPs was determined by recording peak intensities of UV-vis
199 spectra at 400 nm and 520 nm, respectively. The biosensor was optimized with the
200 various aptamer concentrations (METH aptamer: 0, 10, 20, 30, 40, 50, and 60 nM;
201 COC aptamer: 0, 10, 20, 30, 40, and 50 nM).

202 **2.6. Analytical performance evaluation**

203 Under the optimal conditions, we evaluated the sensitivity of the sensor to detect
204 METH by testing various METH concentrations ranging from 0 nM to 200 nM and
205 cocaine from 0 to 150 nM.

206 The selectivity of the sensor was examined by comparing the result with seven
207 common illicit drugs and metabolites, namely cathinone (CAT), methcathinone
208 (MCAT), 3-trifluoromethylphenylpiperazine (BZP), ketamine (KET), morphine
209 (MOR), norketamine (NK), and MDA. The experiment followed the same procedure
210 for the determination of other drugs and metabolites at 1 μ M, the response of which
211 was compared with the signal from METH and cocaine at 50 nM.

212 To explore the performance of our developed biosensors in real applications,
213 effluent wastewater samples (collected from Xiaojiahe Wastewater Plant in Beijing,
214 China) were filtered with 0.22 μ m microporous membrane to remove suspended
215 particulate matter (SPM), followed by spiking METH and cocaine into the wastewater
216 for a final concentration at 75 nM. Spiked wastewater was detected by our biosensor.

217 **2.7. Non-negative matrix factorization (NMF) analysis**

218 “Multiplicative” iteration rules-based NMF was a multi-variant analytical system
219 by non-negative constraints for the generation of the approximate data and application
220 in an analytical science (Berry et al., 2007; Xie et al., 2011). The principle of NMF
221 analysis that processed the UV-vis spectra in this experiment as shown in Figure 1:
222 Given one initial non-negative matrix (V), it could find two different non-negative

223 matrices to approximate the original matrix. The one was the basis matrix (W) and the
224 other one was the coefficient matrix (H). When conducting data analysis, all UV-vis
225 spectra were combined to form matrix V . The number of factors would be set as 2 due
226 to that two nanoparticles (Au@Ag and AuNPs) existed in the solution. Low-rank
227 matrices H and W automatically started from random matrices and stopped while the
228 matrix doesn't change for 10,000 iterations. Matrix H corresponded to the intensity
229 coefficient and W corresponded with the basic spectra for pure Au@Ag NPs and
230 AuNPs. UV-vis spectra results were exported from the instrument software and
231 imported into MATLAB where NMF data processing was performed to directly
232 quantify of METH and COC.

233 **3. Results and discussion**

234 **3.1. Colorimetric sensing principal for METH and cocaine**

235 The AuNPs and Au@Ag NPs were synthesized and characterized by UV-vis
236 spectrometer, SEM and HR-TEM. As shown in Figure 2, AuNPs and Au@Ag NPs
237 were approximately 40 nm with a uniform size (Figure 2b and Figure 2c). Figure 2 (d)
238 indicated a thinner silver layer surrounds the gold core because of the different
239 contrast between these two materials. Figure 2a demonstrated that the UV-vis spectra
240 of Au@Ag NPs and AuNPs. The UV-vis signal peaks of Au@Ag and AuNPs were
241 400 nm and 520 nm, respectively. Compared with the absorption peak of AuNPs, the
242 peak of Au@Ag NPs solution was blue-shifted because Au@Ag NPs and AuNPs
243 with the same particle size had different surface plasmon resonance (SPR)
244 frequencies. This will facilitate to reduce the interference caused by the overlapping
245 peaks when simultaneously detecting cocaine and METH.

246 The working principle of our colorimetric biosensor was shown in Scheme 1. We
247 tried to design two MBs-modified capture probe (CPs), one AuNPs and the other

248 Au@Ag NPs labelled reporter probe (RPs), and two aptamers which specifically
249 bound with METH and COC, respectively. The CPs were superparamagnetic MBs
250 with a carboxyl coating, and it would facilitate sample separation when activated by
251 an external magnetic field. These MBs were functionalized with aminated
252 oligonucleotides (CP DNA) with EDC·HCl as the linker, which could match fully one
253 part of target sequence but different from the fragment complementary with RP DNA
254 (see Figure S1B). The RPs were either Au@Ag NPs or AuNPs modified with RP
255 DNA sequence which is partially complementary to the aptamer. Herein, each
256 aptamer was complementary with its respective MB-conjugated CP DNA and
257 nanoparticle-conjugated RP DNA, then forming a NPs-dsDNA-MBs sandwich
258 structure, for both METH and cocaine.

259 To establish the multiplexed sensors for METH and COC determination, the
260 mixtures in solution containing METH RP, METH CP, COC RP, and COC CP, and
261 two DNA aptamers for illicit drugs were introduced into the solution. After the
262 hybridization, an external magnetic field was able to adsorb the MBs-conjugated
263 complexes, leading to the bound metal nanoparticle decreasing and color changes in
264 the supernatant. However, in the presence of the target drugs, NPs-dsDNA-MBs
265 sandwich structure complex can't be generated because of higher affinity between the
266 aptamer and the target than that from DNA-DNA hybridization. Furthermore, the
267 color of the supernatant depended on the amount of two illicit drugs added to the
268 solution. This interesting color change was useful for simultaneous determination of
269 two targets from a single assay, enabling a novel colorimetric approach for the
270 determination of two illicit drugs. Furthermore, this determination strategy avoided
271 the aggregation between optical noble nanoparticles and the sedimentation, which
272 would be beneficial to minimize the non-specific interference response. Due to that

273 this method only affected the peak intensity rather than the peak position, the UV-vis
274 spectra signal featured an inherent simplicity for quantification.

275 3.2. Detection conditions optimization

276 We optimized a range of detection parameters to improve the sensitivity of our
277 sensors, including the concentration of MBs, the binding time to generate NPs-
278 dsDNA-MBs structure and the aptamer concentration. The optimized concentration of
279 the MBs was determined to be $66.7 \mu\text{g L}^{-1}$, showing in Figure S2. The results also
280 suggested that the concentration of magnetic beads used to remove AuNPs is the same
281 as that of Au@Ag.

282 The reaction time for the formation of NPs-dsDNA-MB was an important
283 parameter for the evaluation of our sensors. Aptamers were introduced and the time
284 set as 0 minutes, and the spectra signal changes are observed. The maximum
285 absorption value of METH and cocaine (Figure S3) were recorded after the addition
286 of DNA aptamers against METH and cocaine, respectively. The incubation was
287 maintained at 25 °C for 110 minutes. Figure S3 demonstrated that the intensity of the
288 UV-vis signal gradually decreased after the addition of the aptamer, and had a
289 minimum value at 60 minutes. Therefore, we used the optimized 60 minutes for our
290 assay.

291 The optimal concentration of DNA aptamers to quench the UV-vis signal of
292 Au@Ag NPs and AuNPs were detected by obtaining absorbance intensities at 400 nm
293 and 520 nm, respectively. Analysis of the plots in Figure S3c showed that the UV-vis
294 signal of AuNPs decreased with increasing METH aptamer concentrations and nearly
295 complete quenching occurred over 60 nM. In this process, it should be noted that if
296 there is excessive METH aptamers, it may result in non-specific (i.e., no surface
297 plasmon resonance enhancement) binding of the aptamer to the METH. As a result,

298 40 nM METH aptamer was optimized in this biosensor. Importantly, we observed
299 METH obviously blocking of the quenching of the AuNPs by 40 nM aptamer,
300 returning the UV-vis intensity of Au@Ag NPs up to 89.1% compared with its initial
301 value (Figure S3c). Similarly, 30 nM cocaine aptamer was optimized and chosen for a
302 sensitive assay (Figure S3d).

303 3.3. Determination of single illicit drug with our sensors

304 To check the feasibility of the sensing platform, the single-target model was firstly
305 to test in our experiment. Firstly, the effects of this analytical method without or with
306 METH, on the UV-vis signal of AuNPs nanoparticles were determined. As shown in
307 the result, in a control experiment, stronger absolute absorbance intensity was
308 observed (Figure 3a, MBs + AuNPs). When METH is introduced, the signal intensity
309 of absorbance had no significant change (Figure 3a, MBs + AuNPs + METH), which
310 indicated that only METH alone had almost no interference to this assay. However,
311 once the addition of METH aptamer in the solution, the signal intensity of absorbance
312 decreased dramatically (Figure 3a, MBs +AuNPs + Apt), due to the formation of the
313 AuNPs-dsDNA-MBs sandwich structure according to the base pair matching
314 principle. The complex would subsequently be eliminated by an external magnetic
315 field. The removal of AuNPs nanoparticles decreased the absorbance intensity. When
316 both METH and its corresponding aptamer were present, the absorbance drastically
317 recovered (Figure 3a, MBs + AuNPs + Apt + METH). The signal was a little lower
318 than the absolute absorbance intensity of AuNPs nanoparticles. The increase in signal
319 intensity of UV-vis spectra with both METH and METH aptamer was due to the
320 formation of METH-aptamer complex, which prevented the formation of the
321 sandwich structure complex and therefore prevented the external magnetic field from
322 removing the AuNPs nanoparticles. Similarly, in the absence of cocaine, Au@Ag NPs

323 can hybridize with aptamer to form a sandwich structure through DNA-DNA
324 hybridization (Figure 3b, MBs + Au@Ag + Apt). When using an external magnetic
325 field, the original deep yellow colour of the supernatant became light yellow.
326 However, when introducing cocaine into the solution, the absorbance was drastically
327 recovered and confirmed that it's the presence (Figure 3c, MBs + Au@Ag + Apt +
328 COC). Hence, the color change of supernatant by certain illicit drugs demonstrated
329 that it was feasible to use the platform for the duplexed determination of illicit drugs.

330 The intensity of peaks at 520 nm assigned to UV-vis signal from AuNPs clearly
331 increased with the addition of the METH. Figure 3c showed the linear fit of the signal
332 intensity of the supernatant solution as the function of the concentration of METH.
333 The linear range for the detection of METH spanned from 1.0 to 200 nM under
334 optimized condition. In similar way, when the concentration of cocaine increased, the
335 signal intensity of the peak at 400 nm associated with Au@Ag NPs increase
336 noticeably (Figure 3d), which led to the colour change of the supernatant solution
337 from light yellow to deep yellow different from other reported colorimetric illicit drug
338 detection method (Shi et al., 2015). The UV-vis spectra signal demonstrated a good
339 linear change ranging from 10 nM to 150 nM.

340 **3.4. Duplexed detection of illicit drugs in a single assay using NMF analysis**

341 Simultaneous determination of different illicit drugs (METH and cocaine) in a
342 single assay was performed through our biosensors. There were two directions of
343 colour conversion (from orange to yellow or red) in this method, our biosensor thus
344 enabled to run a single assay for the determination of two targets. We evaluated the
345 feasibility of our biosensors for the determination of both METH and cocaine in a
346 single assay and the analytical performance from colour changes. A 5×5 matrix was
347 designed in a microplate, in which each element is a sample containing the different

348 concentrations of METH and cocaine. Figure 4b presented the 5×5 matrix photo
349 showing the colour change of two illicit drugs at different concentrations in each
350 microplate. Obviously, the colour change had a significant difference, and varied from
351 5-200 nM for METH and 1-150 nM for cocaine. Also, the performance of the double-
352 colour analytical system was evaluated by UV-vis spectra measurements by
353 constructing a 10×10 matrix varied from 0-200 nM for METH and 0-150 nM for
354 cocaine, respectively. As shown in Figure 4a, both the absorption peaks of UV-vis
355 simultaneously increased when the sample containing both METH and cocaine was
356 introduced. However, the UV-vis spectra of solutions cannot be analyzed as easily as
357 the visual signals due to the interference and overlap between UV-vis spectra of
358 Au@Ag NPs and AuNPs. One of the reasons for such interference is that the UV-vis
359 signal-active nanoparticles are not narrow enough to remove the spectra overlap,
360 which may make it difficult to quantify it. To clearly analyze the UV-vis spectra signal
361 and quantify the METH and cocaine, we made full use of NMF to factorize a series of
362 experimental result and data into two basic data groups.

363 The concentrations of AuNPs and Au@Ag were proportional to the
364 concentrations of the two corresponding illicit drugs. Therefore, the simultaneous
365 quantification of two illicit drugs would be feasible through measuring the UV-vis
366 spectra of these two noble metal nanoparticles. Through NMF analysis, we
367 established a single quantitative analysis for two illicit drugs that worked even when it
368 was difficult to quantify the targets in a complex sample because of the overlap of the
369 two spectra. The target concentrations were quantified by analyzing the changes in the
370 intensity of the signals of UV-vis spectra acquired by NMF. The interference of the
371 spectral overlap between different UV-vis spectra-active nanoparticles could be
372 solved automatically and easily through this data process system. The multivariate

373 evaluation scheme used in this assay could reduce the interference of spectral overlap
374 on the scale of the whole UV-vis spectra rather than just a single peak as in their
375 univariate counterparts. By using the relative intensities of the maximum peak
376 intensity of Au@Ag NPs and AuNPs acquired from NMF, the results clearly
377 demonstrated the real intensities of optical biosensor instead of the overlapping
378 spectra (Figure S4). Figure S5 showed the quantitative result of the multiplexed
379 determination of illicit drugs with two-colour colorimetry, which was almost in accord
380 with Figure 3c and Figure 3d. Although the results verified the validity of the NMF
381 system, the data before and after the NMF process echoed with each other and
382 confirmed the feasibility of undisturbed linear analysis. As shown in Figure S5, the
383 limit of detection (LOD) of METH was determined to be 0.5 nM, whereas the LOD of
384 cocaine was 3.3 nM. The LOD of METH and cocaine were both lower than some
385 previous reports (METH 50 nM (Shi et al., 2015) and cocaine 10 nM (Nie et al.,
386 2013)), respectively, further illustrating the high sensitivity of our proposed approach.

387 In the presence of 7 illicit drugs and metabolites (1 μ M) other than METH,
388 absorbance signals were nearly as low as that from the blank. Meanwhile, these
389 signals were much lower than that with METH and cocaine, though the
390 concentrations of all the other illicit drugs and metabolites were much higher than 50
391 nM METH. What's more, compared with the blank the enhancement in absorbance
392 intensity was not statistically significant among other illicit drugs, indicating that
393 interference of these drugs to METH and cocaine determination was not specific
394 (Figure 5a), which demonstrated that the affinity of illicit drug to certain
395 corresponding aptamer was much better and higher than all other illicit drugs,
396 rendering color array with wonderful specificity toward METH and cocaine. Taking
397 into account the complex matrix of wastewater samples, if we want to use the

398 biosensor for evaluation the pattern of illicit drugs of abuse for WBE, it's worthwhile
399 testing a large cohort of samples to for the calibration curves and improve reliability
400 of our sensors

401 **3.5 Analysis of illicit drugs in wastewater with our biosensors**

402 To evaluate the ability of our colorimetric method for complex sample
403 (wastewater) detection, we used our biosensors for the determination of METH (75
404 nM nominal concentration) and cocaine (75 nM nominal concentration) spiked into
405 the wastewater samples. As shown in Figure 5b, the result we detected for the colour
406 signal intensity of wastewater with cocaine and METH was very much close to that
407 from the buffer, while wastewater without cocaine and METH were all under the
408 threshold value, indicating a negligible matrix effect on our sensing platform.
409 Compared with the measured concentration and real concentration of illicit drugs, the
410 average recovery of METH and COC in spiked effluent wastewater sample are 85.5%
411 and 83.9%, respectively. The results showed great potential for our sensors for the
412 multiplexed determination of illicit drugs in wastewater to evaluate of illicit drug
413 consumption at the community level.

414 **4. Conclusions**

415 In summary, we have described non-aggregated noble metal nanoparticles (AuNPs
416 and Au@Ag) based colorimetric method for the sensitive determination of illicit drugs
417 using METH and cocaine determination as a case study. The biosensor consisted of
418 RPs, CPs, and illicit drug-binding DNA aptamers, where the DNA aptamer could
419 hybridize with both RP and CP, generating NPs-dsDNA-MBs sandwich structure.
420 When an external magnetic field is used, the sandwich structure was removed from
421 the solution, leading to the absorbance intensity decreasing. The absorbance intensity
422 was correlated with the concentrations of illicit drugs, enabling the quantification of

423 the drugs. To solve the spectral overlap in this sensing platform, the information of
424 supernatant was used for the quantification of multiplexed targets with an NMF
425 analysis. Through an automatic NMF analysis, our colorimetric biosensors provided a
426 simple and rapid quantification platform for two illicit drugs analysis at nM level in a
427 single assay. These results showed that our proposed sensors have a huge potential on
428 estimating the consumption of illicit drugs for WBE.

429 There is a growing requirement to monitor illicit drugs and other emerging
430 contaminants in wastewater. Aptamers are synthetic single-stranded DNA which can
431 specifically bind to a wide range of respective targets with a promising selectivity and
432 sensitivity. This will enable our proposed biosensors to be used as a generic platform
433 to detect a variety of contaminants by simply replacing certain corresponding
434 aptamers, and easy to be improved from duplex assay to highly multiplexed
435 determination for a range of substances. To obtain a reliably detection, it was
436 suggested to test a large cohort of wastewater sample with a proper validation method.
437 We believe that the rapid sensors will play an increasing role of monitoring of illicit
438 drug of abuse and contribute as an alternative way for WBE.

439 **Acknowledgment**

440 We thank for NSFC grant (No. 41371442 and 41401566). ZY thanks UK NERC
441 Fellowship grant (NE/R01334 9/1).

442 **References**

- 443 Asghary M, Raoof JB, Rahimnejad M, Ojani R. Microbial fuel cell-based self-powered biosensing
444 platform for determination of ketamine as an anesthesia drug in clinical serum samples.
445 *Journal of the Iranian Chemical Society* 2018; 15: 445-453.
- 446 Bade R, Tschärke BJ, White JM, Grant S, Mueller JF, O'Brien J, et al. LC-HRMS suspect screening to
447 show spatial patterns of New Psychoactive Substances use in Australia. *Science of The Total*
448 *Environment* 2019; 650: 2181-2187.
- 449 Berry MW, Browne M, Langville AN, Pauca VP, Plemmons RJ. Algorithms and applications for
450 approximate nonnegative matrix factorization. *Computational Statistics and Data Analysis*
451 2007; 52: 155-173.
- 452 Castrignanò E, Yang Z, Bade R, Baz-Lomba JA, Castiglioni S, Causanilles A, et al. Enantiomeric
453 profiling of chiral illicit drugs in a pan-European study. *Water Research* 2018; 130: 151-160.

454 Cyranoski D. China expands surveillance of sewage to police illegal drug use. *Nature* 2018; 559: 310-
455 311.

456 Du P, Li K, Li J, Xu Z, Fu X, Yang J, et al. Methamphetamine and ketamine use in major Chinese
457 cities, a nationwide reconnaissance through sewage-based epidemiology. *Water Research*
458 2015; 84: 76-84.

459 Du P, Zhou Z, Bai Y, Xu Z, Gao T, Fu X, et al. Estimating heroin abuse in major Chinese cities
460 through wastewater-based epidemiology. *Science of The Total Environment* 2017; 605-606:
461 158-165.

462 Du P, Zhou Z, Huang H, Han S, Xu Z, Bai Y, et al. Estimating population exposure to phthalate esters
463 in major Chinese cities through wastewater-based epidemiology. *Science of The Total*
464 *Environment* 2018; 643: 1602-1609.

465 EMCDDA. Assessing illicit drugs in wastewater: advances in wastewater-based drug epidemiology.
466 2016.

467 Ettore Z, Chiara C, Sara C, Renzo B, Roberto F. Estimating community drug abuse by wastewater
468 analysis. *Environ Health Perspect* 2008; 116: 1027-1032.

469 Foppe KS, Hammond-Weinberger DR, Subedi B. Estimation of the consumption of illicit drugs during
470 special events in two communities in Western Kentucky, USA using sewage epidemiology.
471 *Science of The Total Environment* 2018; 633: 249-256.

472 Galanie S, Thodey K, Trenchard IJ, Filsinger Interrante M, Smolke CD. Complete biosynthesis of
473 opioids in yeast. *Science* 2015; 349: 1095-1100.

474 Gao T, Du P, Xu Z, Li X. Occurrence of new psychoactive substances in wastewater of major Chinese
475 cities. *Science of The Total Environment* 2017; 575: 963-969.

476 Kumar V, Kumar P, Pournara A, Vellingiri K, Kim K-H. Nanomaterials for the sensing of narcotics:
477 Challenges and opportunities. *TrAC Trends in Analytical Chemistry* 2018; 106: 84-115.

478 Li K, Qin W, Li F, Zhao X, Jiang B, Wang K, et al. Nanoplasmonic Imaging of Latent Fingerprints and
479 Identification of Cocaine. *Angewandte Chemie* 2013; 125: 11756-11759.

480 Lodha A, Pandya A, Sutariya PG, Menon SK. A smart and rapid colorimetric method for the detection
481 of codeine sulphate, using unmodified gold nanoprobe. *RSC Advances* 2014; 4: 50443-50448.

482 Mao K, Yang Z, Du P, Xu Z, Wang Z, Li X. G-quadruplex-hemin DNzyme molecular beacon probe
483 for the detection of methamphetamine. *RSC Advances* 2016; 6: 62754-62759.

484 Mao K, Zhou Z, Han S, Zhou X, Hu J, Li X, et al. A novel biosensor based on Au@Ag core-shell
485 nanoparticles for sensitive detection of methylamphetamine with surface enhanced Raman
486 scattering. *Talanta* 2018; 190: 263-268.

487 Merz F. United Nations Office on Drugs and Crime: World Drug Report 2017. 2017. SIRIUS -
488 *Zeitschrift für Strategische Analysen*. 2, 2018, pp. 85.

489 Mokhtarzadeh A, Ezzati Nazhad Dolatabadi J, Abnous K, de la Guardia M, Ramezani M.
490 Nanomaterial-based cocaine aptasensors. *Biosensors and Bioelectronics* 2015; 68: 95-106.

491 Neves MAD, Blaszykowski C, Bokhari S, Thompson M. Ultra-high frequency piezoelectric aptasensor
492 for the label-free detection of cocaine. *Biosensors and Bioelectronics* 2015; 72: 383-392.

493 Nie J, Zhang D-W, Tie C, Zhou Y-L, Zhang X-X. A label-free DNA hairpin biosensor for colorimetric
494 detection of target with suitable functional DNA partners. *Biosensors and Bioelectronics*
495 2013; 49: 236-242.

496 Roncancio D, Yu H, Xu X, Wu S, Liu R, Debord J, et al. A Label-Free Aptamer-Fluorophore
497 Assembly for Rapid and Specific Detection of Cocaine in Biofluids. *Analytical Chemistry*
498 2014; 86: 11100-11106.

499 Shen A, Chen L, Xie W, Hu J, Zeng A, Richards R, et al. Triplex Au-Ag-C Core-Shell Nanoparticles
500 as a Novel Raman Label. *Advanced Functional Materials* 20 2010: 969-975.

501 Shi Q, Shi Y, Pan Y, Yue Z, Zhang H, Yi C. Colorimetric and bare eye determination of urinary
502 methylamphetamine based on the use of aptamers and the salt-induced aggregation of
503 unmodified gold nanoparticles. *Microchimica Acta* 2015; 182: 505-511.

504 Song E, Han W, Li J, Jiang Y, Cheng D, Song Y, et al. Magnetic-Encoded Fluorescent Multifunctional
505 Nanospheres for Simultaneous Multicomponent Analysis. *Analytical Chemistry* 2014; 86:
506 9434-9442.

507 Stojanovic MN, De PP, Landry DW. Fluorescent Sensors Based on Aptamer Self-Assembly. *Journal of*
508 *the American Chemical Society* 2000; 122: 11547-11548.

509 Tang D, Wang Q, Wang Z, Liu Q, Zhang B, He D, et al. Highly sensitive wearable sensor based on a
510 flexible multi-layer graphene film antenna. *Science Bulletin* 2018; 63:574-579.

511 Thomas KV, Bijlsma L, Castiglioni S, Covaci A, Emke E, Grabic R, et al. Comparing illicit drug use in
512 19 European cities through sewage analysis. *Science of The Total Environment* 2012; 432:
513 432-439.

514 van Nuijs ALN, Castiglioni S, Tarcomnicu I, Postigo C, de Alda ML, Neels H, et al. Illicit drug
515 consumption estimations derived from wastewater analysis: A critical review. *Science of the*
516 *Total Environment* 2011; 409: 3564-3577.

517 Wen C-Y, Wu L-L, Zhang Z-L, Liu Y-L, Wei S-Z, Hu J, et al. Quick-Response Magnetic Nanospheres
518 for Rapid, Efficient Capture and Sensitive Detection of Circulating Tumor Cells. *ACS Nano*
519 2014; 8: 941-949.

520 Xie W, Herrmann C, Kömpe K, Haase M, Schlücker S. Synthesis of Bifunctional Au/Pt/Au Core/Shell
521 Nanoraspberries for in Situ SERS Monitoring of Platinum-Catalyzed Reactions. *Journal of the*
522 *American Chemical Society* 2011; 133: 19302-19305.

523 Xu Z, Du P, Li K, Gao T, Wang Z, Fu X, et al. Tracing methamphetamine and amphetamine sources in
524 wastewater and receiving waters via concentration and enantiomeric profiling. *Science of The*
525 *Total Environment* 2017; 601-602: 159-166.

526 Ya Y, Yifeng T, Xiaoshu W, Jinyin P, Yun D. A label-free immunosensor for ultrasensitive detection
527 of ketamine based on quartz crystal microbalance. *Sensors* 2015; 15: 8540-9.

528 Yang Z, Castrignanò E, Estrela P, Frost CG, Kasprzyk-Hordern B. Community Sewage Sensors
529 towards Evaluation of Drug Use Trends: Detection of Cocaine in Wastewater with DNA-
530 Directed Immobilization Aptamer Sensors. *Scientific Reports* 2016; 6: 21024.

531 Zuccato E, Chiabrando C, Castiglioni S, Calamari D, Bagnati R, Schiarea S, et al. Cocaine in surface
532 waters: a new evidence-based tool to monitor community drug abuse. *Environmental Health*
533 2005; 4: 14.

534

Highlights

- We developed a novel nanoparticles-based biosensor for the detection of illicit drugs.
- High selective and sensitive detection of two illicit drug (LOD of METH is 0.5 nM and cocaine is 3.3 nM) in a single assay.
- The biosensor enables a generic platform for the detection of illicit drugs in wastewater.

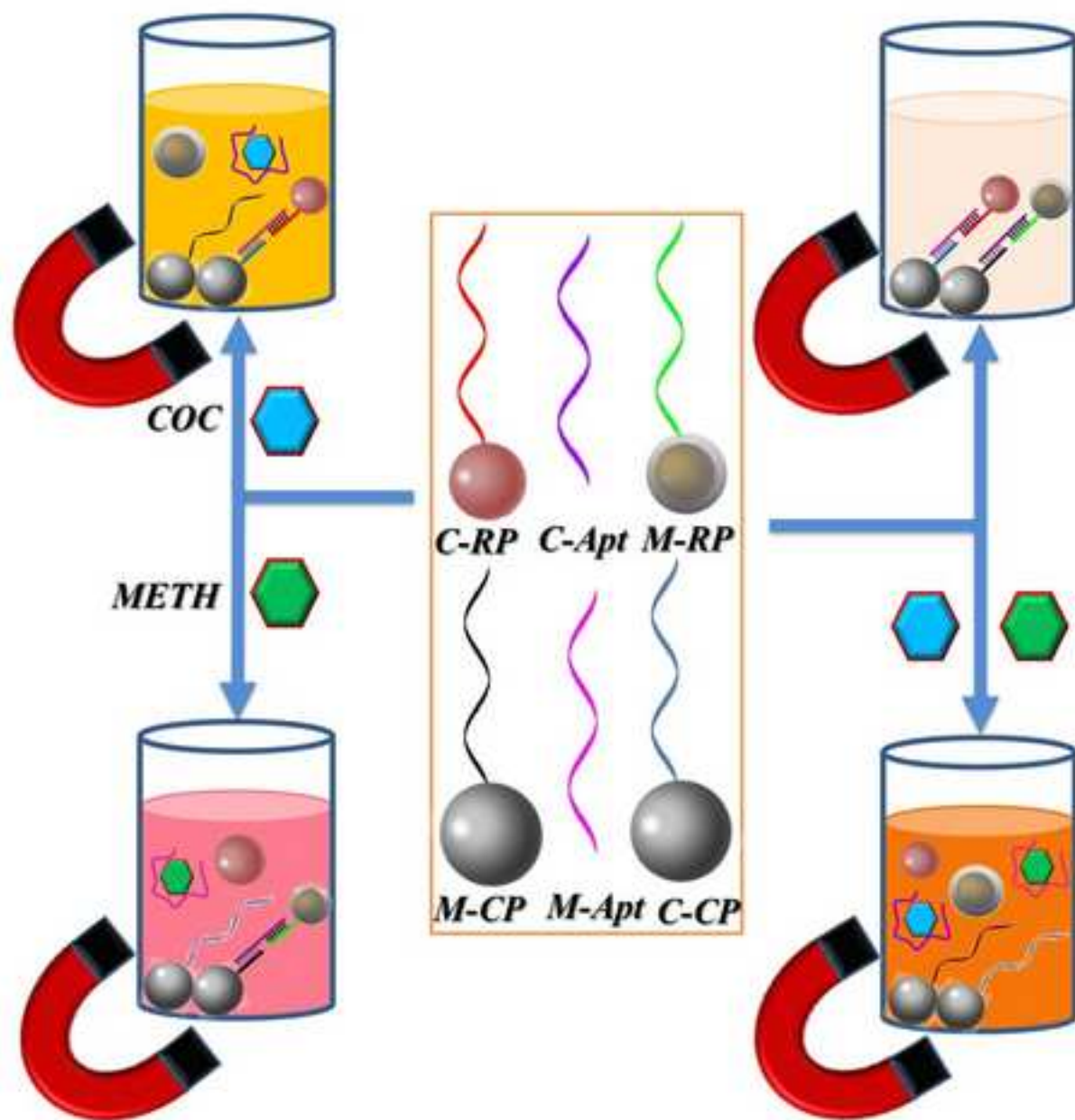
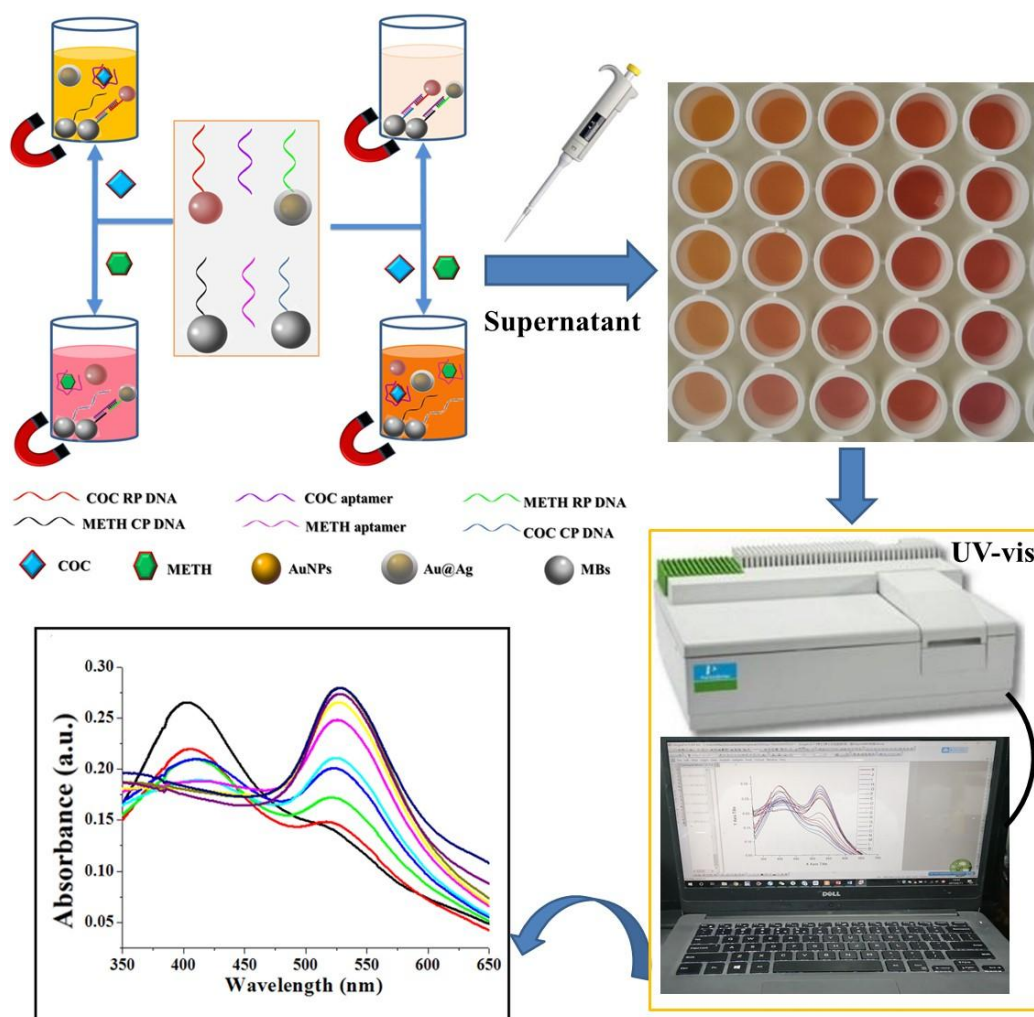


Figure captions:



Scheme 1. Schematic illustration of colorimetric detection of METH and cocaine based on non-aggregated nanoparticles (C-RP: cocaine reporter probe, M-RP: methamphetamine reporter probe, M-CP, methamphetamine capture probe, and C-CP: cocaine capture probe).

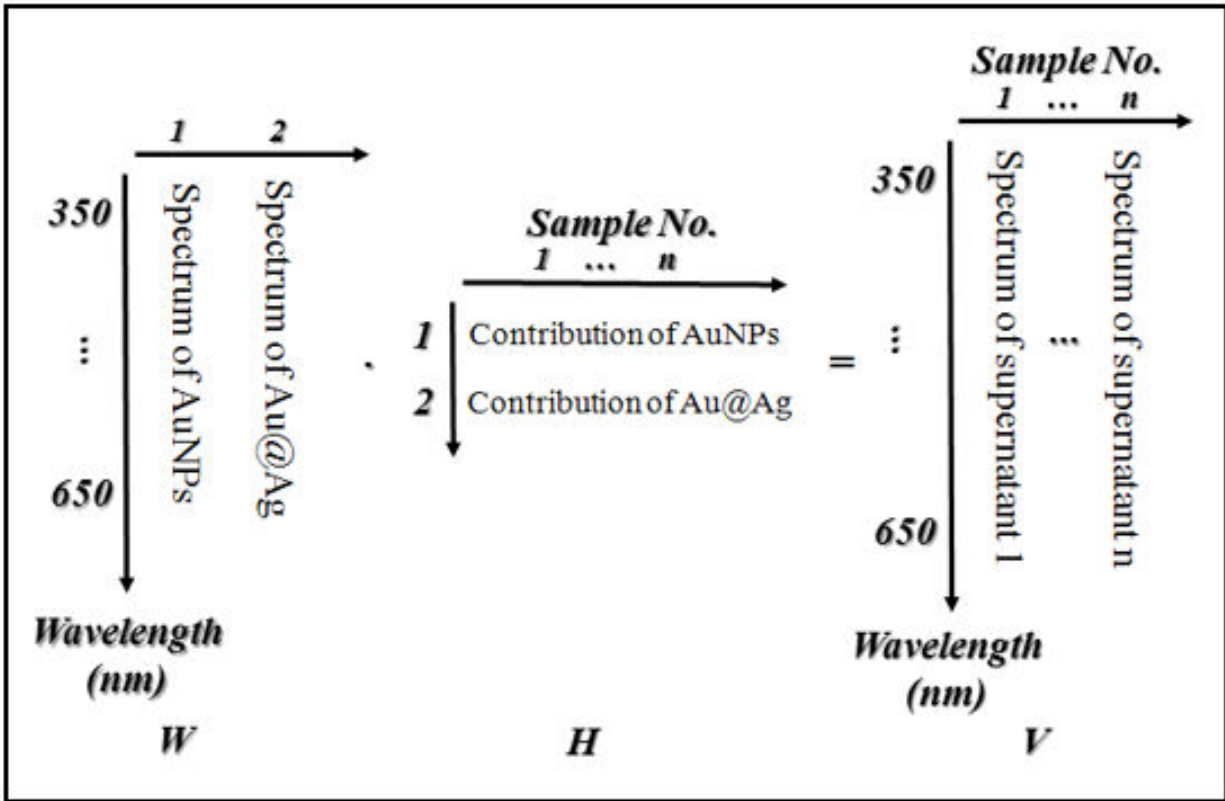


Figure 1. The principle of NMF analysis that processes the UV-vis spectra.

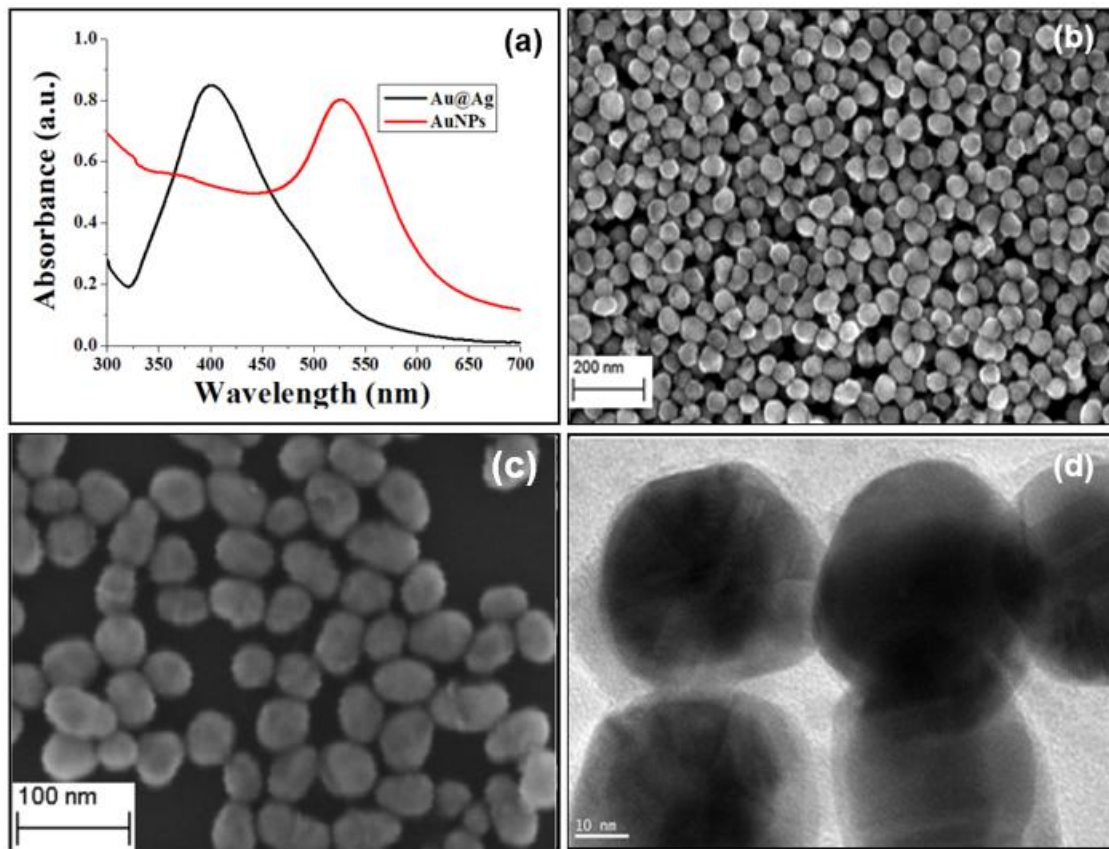


Figure 2. (a) UV-vis spectra of Au@Ag and AuNPs; (b) SEM image of AuNPs; (c) SEM image and (d) high resolution transmission emission microscope (HR-TEM) image of Au@Ag core-shell nanoparticles.

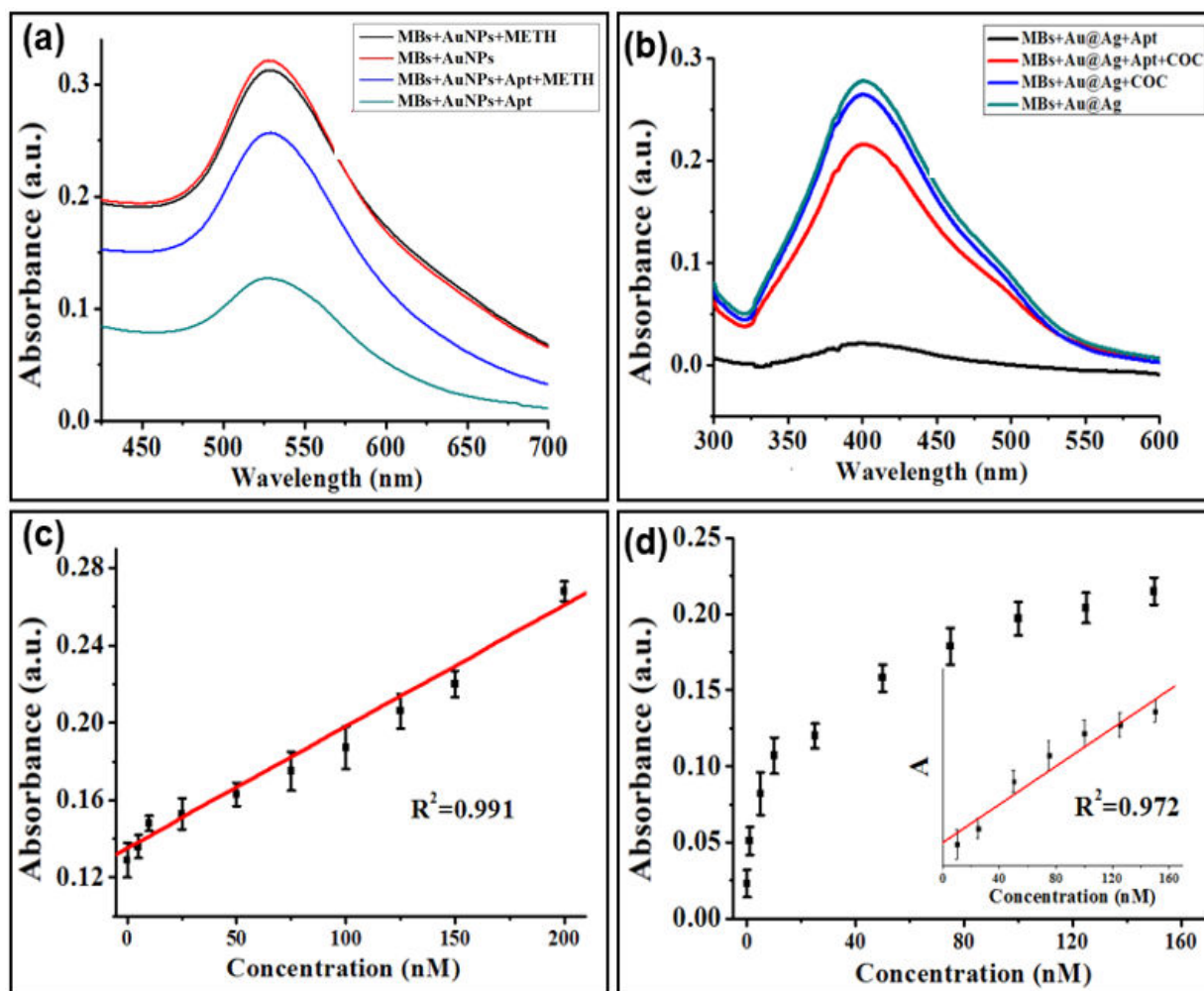


Figure 3. (a) UV-vis spectra of AuNPs in the presence of METH and control experiment; (b) UV-vis spectra of Au@Ag in the presence of COC and control experiment; (c) METH concentration-dependent change of SPR signal intensity ($\lambda_{\max}=520$ nm) from 0 to 200.0 nM; (d) COC concentration-dependent change of SPR signal intensity ($\lambda_{\max}=400$ nm) from 0 to 150.0 nM. The inset shows the linear range concentration from 10.0 to 150.0 nM, error bar representing at least three independent measurements.

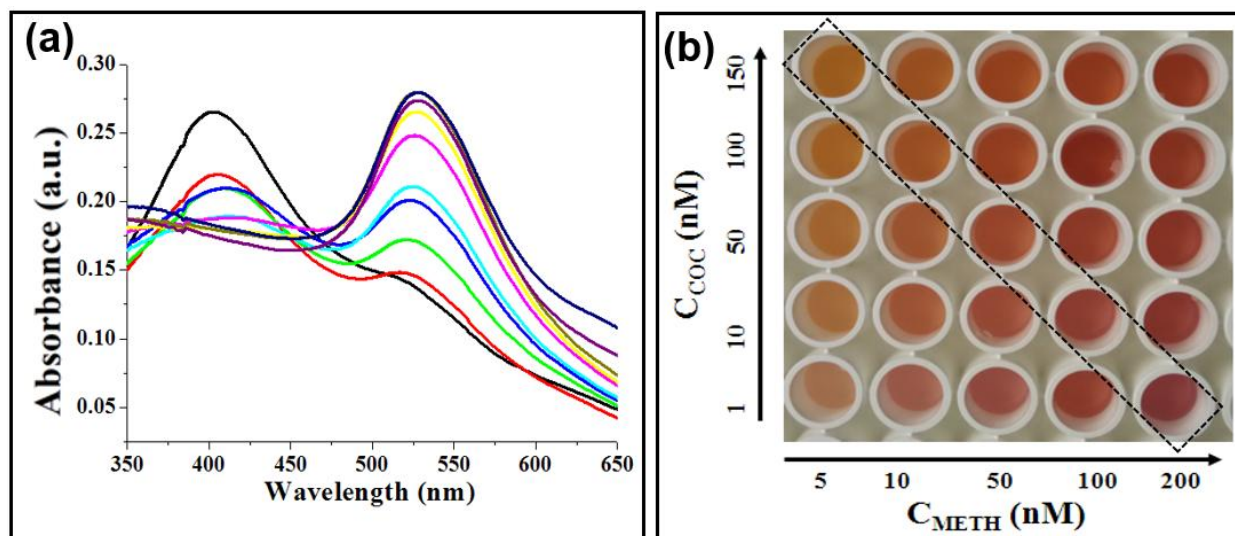


Figure 4. (a) UV-vis spectra of supernatant with the presence of different concentrations of METH and COC after incubation at 25 °C for 60 min (COC from bottom to top: 0, 1, 5, 10, 25, 50, 75, 100, 125, and 150 nM; METH from bottom to top: 0, 5, 10, 25, 50, 75, 100, 125, 150, and 200 nM.). (b) Photograph displaying the color change of the supernatant mixtures with different concentrations of targets (COC from bottom to top: 1, 10, 50, 100, and 150 nM; METH from left to right: 5, 10, 50, 100, and 200 nM).

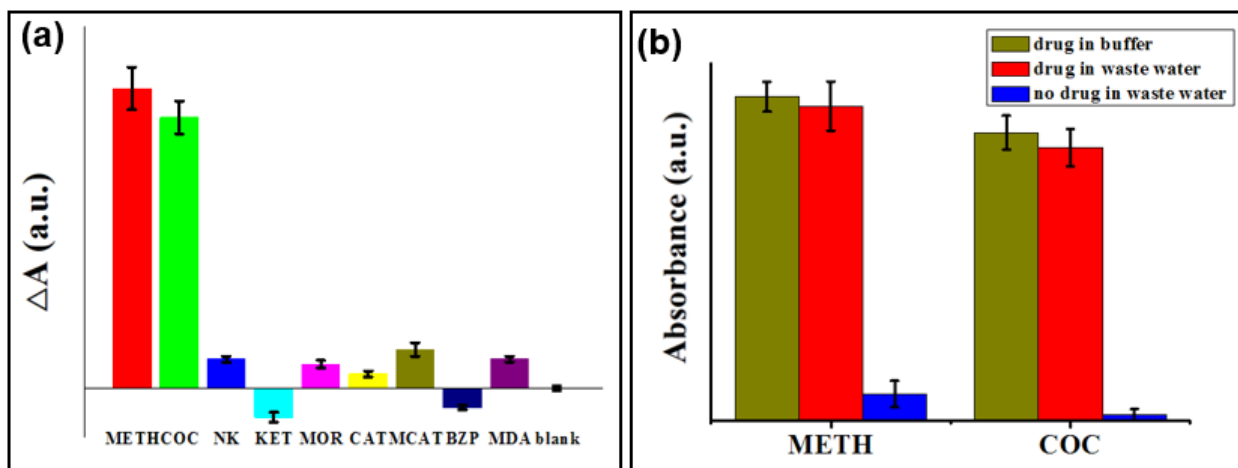


Figure 5. (a) Selectivity of the non-aggregation nanoparticles for METH and COC detection. The METH and COC concentration was 50 nM, while the concentrations of other illicit drugs were 1 μ M, METH, COC, NK, KET, MOR, CAT, MCAT, BZP, MDA, and blank. (b) Histogram for SPR intensities of METH and COC detection in wastewater. The signal (ΔA) represents the relative absorbance with respect to the blank and error bars represent three independent measurements.